Closing the pressure gap in x-ray photoelectron spectroscopy by membrane hydrogenation

Delmelle, Renaud ; Probst, Benjamin ; Alberto, Roger ; Züttel, Andreas ; Bleiner, Davide ; Borgschulte, Andreas

Abstract: Comprehensive studies of gas-solid reactions require the in-situ interaction of the gas at a pressure beyond the operating pressure of ultrahigh vacuum (UHV) X-ray photoelectron spectroscopy (XPS). The recent progress of near ambient pressure XPS allows to dose gases to the sample up to a pressure of 20 mbar. The present work describes an alternative to this experimental challenge, with a focus on H2 as the interacting gas. Instead of exposing the sample under investigation to gaseous hydrogen, the sample is in contact with a hydrogen permeation membrane, through which hydrogen is transported from the outside to the sample as atomic hydrogen. Thereby, we can reach local hydrogen concentrations at the sample inside an UHV chamber, which is equipped with surface science tools, and this corresponds to a hydrogen pressure up to 1 bar without affecting the sensitivity or energy resolution of the spectrometer. This experimental approach is validated by two examples, that is, the reduction of a catalyst precursor for CO2 hydrogenation and the hydrogenation of a water reduction catalyst for photocatalytic H2 production, but it opens the possibility of the new in situ characterisation of energy materials and catalysts.

DOI: https://doi.org/10.1063/1.4921353

AIP | Review of Scientific Instruments

Closing the pressure gap in x-ray photoelectron spectroscopy by membrane hydrogenation

Renaud Delmelle, Benjamin Probst, Roger Alberto, Andreas Züttel, Davide Bleiner, and Andreas Borgschulte

Citation: Review of Scientific Instruments **86**, 053104 (2015); doi: 10.1063/1.4921353
View online: http://dx.doi.org/10.1063/1.4921353
View Table of Contents: http://scitation.aip.org/content/aip/journal/rsi/86/5?ver=pdfcov
Published by the AIP Publishing

Closing the pressure gap in x-ray photoelectron spectroscopy by membrane hydrogenation

Renaud Delmelle,[1,2] Benjamin Probst,[3] Roger Alberto,[3] Andreas Züttel,[2,4] Davide Bleiner,[1] and Andreas Borgschulte[1,2,a)]

[1]*Laboratory for Advanced Analytical Technologies, Swiss Federal Laboratories for Materials Science and Technology (Empa), Überlandstrasse 129, CH-8600 Dübendorf, Switzerland*
[2]*Laboratory for Hydrogen and Energy, Swiss Federal Laboratories for Materials Science and Technology (Empa), Überlandstrasse 129, CH-8600 Dübendorf, Switzerland*
[3]*Department of Chemistry, University of Zürich (UZH), CH-8057 Zürich, Switzerland*
[4]*Ecole Polytechnique Fédérale de Lausanne (EPFL), SB, ISIC, LMER, CH-1015 Lausanne, Switzerland*

(Received 10 March 2015; accepted 7 May 2015; published online 21 May 2015)

Comprehensive studies of gas-solid reactions require the in-situ interaction of the gas at a pressure beyond the operating pressure of ultrahigh vacuum (UHV) X-ray photoelectron spectroscopy (XPS). The recent progress of near ambient pressure XPS allows to dose gases to the sample up to a pressure of 20 mbar. The present work describes an alternative to this experimental challenge, with a focus on H_2 as the interacting gas. Instead of exposing the sample under investigation to gaseous hydrogen, the sample is in contact with a hydrogen permeation membrane, through which hydrogen is transported from the outside to the sample as atomic hydrogen. Thereby, we can reach local hydrogen concentrations at the sample inside an UHV chamber, which is equipped with surface science tools, and this corresponds to a hydrogen pressure up to 1 bar without affecting the sensitivity or energy resolution of the spectrometer. This experimental approach is validated by two examples, that is, the reduction of a catalyst precursor for CO_2 hydrogenation and the hydrogenation of a water reduction catalyst for photocatalytic H_2 production, but it opens the possibility of the new in situ characterisation of energy materials and catalysts. © *2015 AIP Publishing LLC*. [http://dx.doi.org/10.1063/1.4921353]

I. INTRODUCTION

The understanding of hydrogen–solid interactions is a central scientific challenge in various contexts, such as the development of solid catalysts for water splitting[1] or CO_2 hydrogenation,[2] the study of hydrogen embrittlement,[3] and the investigation of various types of hydrides (i.e., metallic,[4] complex,[5] and organic[6]) for hydrogen detection, permeation, and storage. *In situ* information about chemical bonds and/or the electronic configuration of valence states is of great interest, both in terms of the compounds themselves and their formation/decomposition intermediates. Such information is usually gathered for the bulk compounds, whereas information for their surface counterparts—which are nothing more than the gateways between the gas phase and the bulk of the material—is much more difficult to obtain. X-ray photoelectron spectroscopy (XPS) is a powerful surface characterisation technique, providing insightful information about the elements present on a given surface, including their respective chemical states and concentrations across as many as a few tens of atomic layers. However, the short mean-free path of electrons with energies below 1500 eV in a gas at ambient pressure does not allow XPS analyses to be performed under realistic experimental conditions, from an applications point of view,[7] and a vacuum level is required for X-ray anodes and channeltrons.[8]

These problems can be partly overcome by performing so-called "environmental," "ambient-pressure," or "high-pressure" XPS.[7–12] These techniques rely on the use of differential pumping stages, the minimisation of the specimen–aperture distance in the high-pressure regions, and, for the most recent systems, the addition of electrostatic lenses to focus the electrons through the differential pumping scheme.[8–10] Among the most effective systems available, the pressure in the analysis chamber (AC) can reach a few tens of mbar, with acceptable photoelectron intensity losses.[8–10] Nonetheless, these techniques suffer from drawbacks, such as reduced energy resolution and specimen freedom of movement, high cost, and accessibility to the facilities, as most of them are dedicated for operation at synchrotron light sources. Some laboratory-scale solutions have also been developed recently,[7,11,12] allowing for environmental XPS analyses to be performed with a reduced cost and increased availability. Unfortunately, it has to be concluded that the so-called "pressure gap" in XPS can still only be partially filled with a limited maximum pressure, lower spectrometer resolution, and high cost.

In this work, we propose a new experimental approach to study materials exposed to high hydrogen "pressures" by means of XPS while keeping the analysis chamber, at least, under high vacuum, thereby ignoring the usual drawbacks related to differential pumping. A new type of specimen holder has been designed in this respect, consisting of a metallic membrane fed on one side with a high hydrogen pressure and exposed on the other side to the X-ray beam at ultrahigh vacuum (UHV)-compatible pressures. We show that by choosing materials that exhibit appropriate hydrogen permeation

a)Author to whom correspondence should be addressed. Electronic mail: andreas.borgschulte@empa.ch. Telephone: +41-58-765.4639. Fax: +41-58-765.69.22.

kinetics, monoatomic hydrogen can rapidly be generated at the membrane surface (feed side) and transferred through the bulk to the surface exposed to the vacuum. Moreover, adjusting the membrane composition and temperature as well as the hydrogen partial pressure on the membrane feed side (p_{feed}) allows us to tune the desired hydrogen flux on the membrane surface, depending on the specimen being analysed and the experimental conditions desired. By capping the membrane with a material of interest, we are then able to study hydrogen–solid interactions by means of XPS with realistic hydrogen concentrations.

This new experimental concept will be described in detail. Its performance will then be evaluated, both in terms of hydrogen permeation behaviour and spectrometer sensitivity/resolution. Two example applications of the presented *in situ* XPS approach will then be given, that is, the reduction of a precursor for catalytic CO_2 hydrogenation and the hydrogenation of a water reduction catalyst (WRC).

II. SYSTEM DESIGN

The XPS system described here is mainly dedicated to *in situ* surface analyses of various types of hydride-forming materials in the Laboratory for Hydrogen and Energy at Empa, Switzerland. It primarily consists of three stainless-steel vacuum chambers with mu-metal shieldings: the fast entry lock (FEL), the preparation chamber (PC), and the AC. While the FEL vacuum is ensured by a primary rotary pump (type Alcatel 2012A, maximum water vapour pumping rate: 150 g/h) and a secondary turbo pump (type Pfeiffer HiPace 80, volume flow rate for N_2: 67 l/s), the PC and AC are both continuously connected to a primary rotary pump (type Edwards E2M30, maximum water vapour pumping rate: 0.7 kg/h), to a secondary turbo pump (type Pfeiffer TMU 071, volume flow rate for N_2: 59 l/s), and to a Ti sublimation pump (ZST22 from VG Scienta). The setup design is shown in Fig. 1(a). The base pressures are of the order of 10^{-7} mbar in the FEL, 10^{-9} mbar in the PC, and 10^{-10} mbar in the AC. The pressure is monitored in the FEL, PC, and AC by the following gauges: Pfeiffer PKR 251 (measurement range: 5×10^{-9}–1000 mbar), Pfeiffer IKR 270 (measurement range: 5×10^{-11}–0.01 mbar), and VG Scienta VIG17 (measurement range: 10^{-11}–10^{-3} mbar), respectively.

A. Basic components: Source and detector

The X-ray source used in this setup is a XR3 Twin Anode from Thermo Scientific. Its two active anode faces are coated with Al (E = 1486.8 eV, ΔE = 0.7 eV) and Mg (E = 1253.6 eV, ΔE = 0.85 eV). Both of them can be run with a cross contamination of <0.35%. The anode power can reach 300 W, with a corresponding acceleration voltage and emission current of 15 kV and 20 mA, respectively. Two thoria-coated Ir

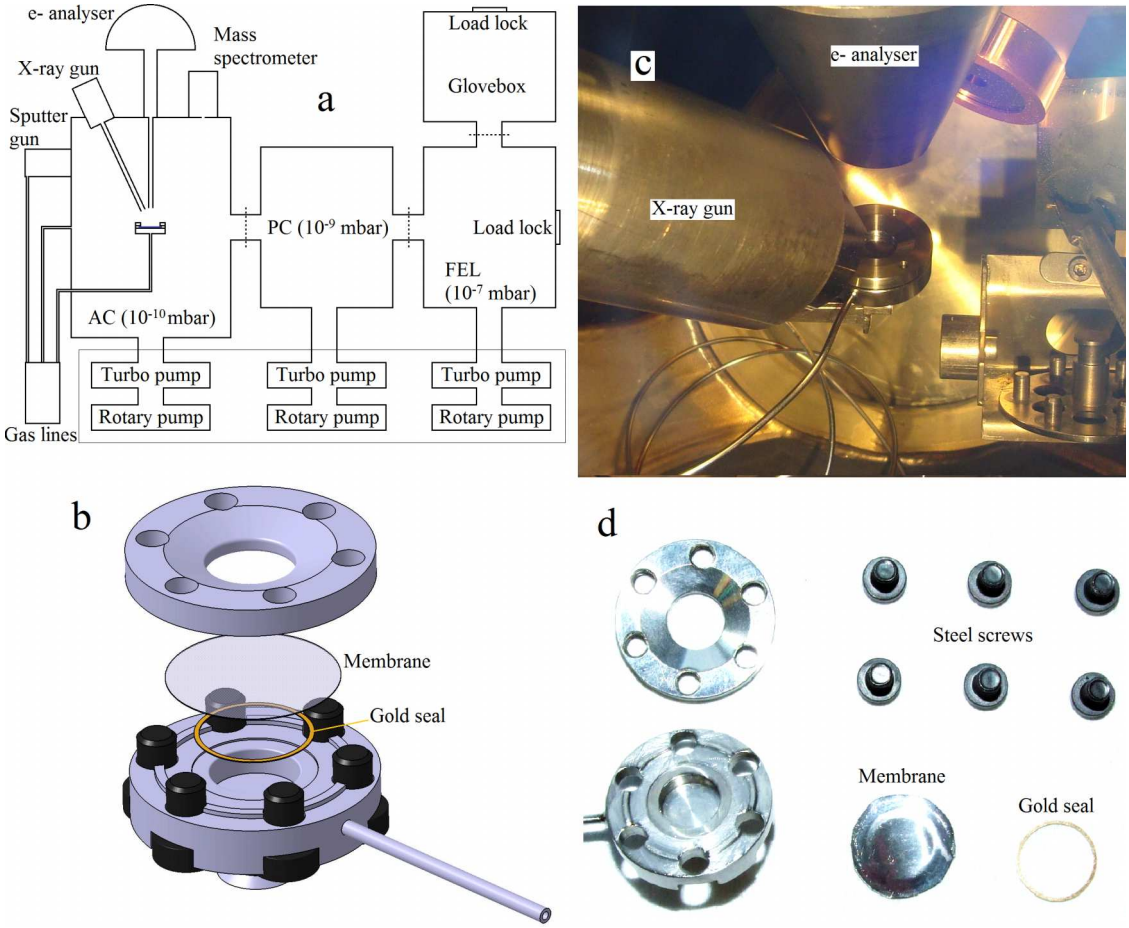

FIG. 1. (a) General scheme of the XPS setup. (b) Scheme of the membrane specimen holder. (c) Photograph of the specimen holder mounted in the AC. (d) Photograph of the spare parts of the membrane specimen holder.

cathodes are used, each one assigned to one of the anode faces. A T-shaped piece located between the X-ray source and the AC allows the direct connection of XR3 to the high-vacuum pumps, allowing a gain of one order of magnitude in terms of pressure tolerance compared to the AC. The analyser is a PHOIBOS 100 Hemispherical Energy Analyser from SPECS. It includes a lens system and a hemispherical energy analyser, both constructed with non-magnetic materials and protected by mu-metal shielding. The analyser is also directly connected to the high-vacuum pumps, providing a pressure that is roughly one order of magnitude better than that in the analysis chamber. It can work in spatially resolved, transmission-optimised, and angular-resolved modes with adjustable slit sizes and acceptance angles. The PHOIBOS 100 is coupled to a HSA 3500 power supply, providing an energy span of ±3500 eV. In the XPS configuration, the pass energy range is 0–100 eV and the minimum energy step width is 1.6 meV. The detector assembly consists of a five-channel electron multiplier arranged as a single compact block, providing high count rates and good durability. In this study, the XPS measurements were carried out in fixed analyser transmission (FAT) mode with a pass energy of 50 eV. The entrance and exit slit sizes were set to 7×20 mm and 20×71 mm, respectively. The XPS data were acquired by SpecsLab software and it were processed by CasaXPS software.[13]

B. Additional components for *in situ* analysis

Additional components are routinely used together with this XPS system for many purposes such as *in situ* specimen cleaning as well as gas–solid interaction, thermal decomposition, and gaseous decomposition product analysis. These components are described herein.

Surface cleaning and depth-profiling analyses are performed with a Penning Ion Source IQP 10/63 from SPECS, mounted in a standard configuration with a 2 mm diameter aperture. The operating gas is ionised at low pressure with electrons generated by a cold cathode, such that the sputtering pressure—adjusted by a standard leak valve—allows the chamber to remain at least in high vacuum (on the order of 10^{-6} mbar in the AC). Discharge currents and voltages are in the 5–10 mA and 600–800 V range, respectively, with an acceleration potential around 5 kV and currents up to 50 μA on the specimen surface.

A second leak valve connected to the AC allows the exposure of the specimen surface to a given gas species at a partial pressure that is acceptable for the pumping system, that is, below 10^{-5} mbar. As will be seen below, a third gas line, working up to atmospheric pressure, can be connected to the new specimen holder developed in this study.

The specimen manipulator (HPT 1 from AG Scienta) allows the specimen holders to be either cooled or heated *in situ*. Cooling is realised with liquid nitrogen, whereas heating of the specimen holder is done by controlling the current passing through a filament with a laboratory power supply (EA-PS 3016-10 B from Elektro-Automatik) combined with a temperature controller (KS 90-1 from PMA), monitoring the specimen temperature with a standard type K thermocouple.

The gaseous species produced during our *in situ* experiments are analysed in real time with a Pfeiffer Prisma QMS 200 quadrupole mass spectrometer. Its measurement range is 10^{-12}–10^{-4} mbar (total pressure in AC) and its sensitivity to Ar is $>1 \times 10^{-3}$ A/mbar. The data produced by this mass spectrometer were acquired by Quadstar software, as was the temperature signal from the thermocouple.

C. Membrane specimen holder

The key element in the conception of this setup lies in the use of a hydrogen-permeable membrane, fed on one side with a high-hydrogen pressure and exposed on the other side to the AC of the XPS system. Figs. 1(b)–1(d) show this membrane design. The design was conceived at the Hydrogen and Energy Department and fabricated at the Mechanical Engineering Department of Empa Dübendorf, Switzerland. The membrane itself is circular with a diameter of 1.5 cm. It is clamped between two steel pieces by six steel screws and sealed by a gold ring. Gold was chosen as it can resist to high temperatures, because the specimen manipulator can be heated, as explained above. Once clamped, the diameters of the membrane surfaces exposed to the AC and to hydrogen are reduced to 9 mm. The feed side is connected to an external gas line by a flexible steel pipe with a diameter of 1 mm. This specimen holder geometry allows the specimen to be manipulated in the same way as it can be with a regular specimen holder. Furthermore, it also allows the membrane to be replaced easily, which can then be coated with any hydride-forming material. Therefore, if one chooses the appropriate material (see Sec. III), the membrane can serve as a hydrogen-providing surface that is directly in contact with the specimen of interest. As monoatomic hydrogen is directly transferred between the membrane and the specimen, the AC can remain in UHV (at least in high vacuum when hydrogen is permeating through the membrane). The membranes presented here are standard metal foils from Goodfellow.

The main drawback of this specimen holder is that the XPS system has to be vented in order to replace the membrane, because it is connected to a gas line. Unlike the gas lines to the sputtering system and the AC leak valve, the third gas line can be flushed independently using a rotary pump (type Edwards RV12, maximum water vapour pumping rate: 0.06 kg/h). The use of an independent pumping scheme was chosen in order to be able to efficiently flush the membrane feed side in case of membrane failure, which would cause a direct leak into the AC. The pressure in this gas line is continuously monitored with an electronic gauge (Pfeiffer CMR 361; measurement range: 0.1–1100 mbar) in order to quantify the hydrogen flux going through the membrane.

III. PROOF OF PRINCIPLE AND SYSTEM PERFORMANCE

The basic idea of the measurement method stems from the special conditions required for a functioning (hydrogen) membrane:

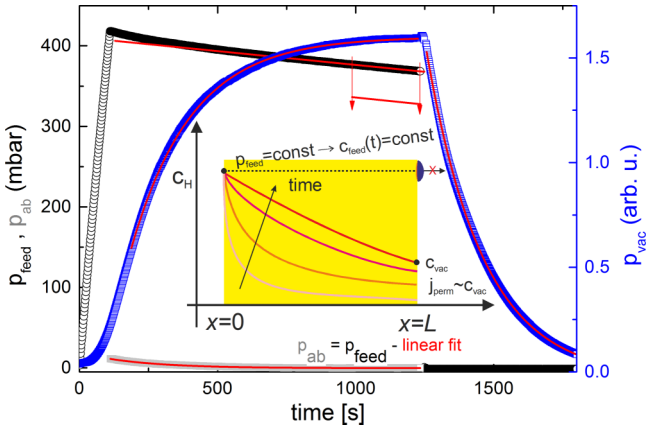

FIG. 2. Time evolution of p_{vac} after setting p_{feed} to 420 mbar, with the derivation of p_{ab}. Inset: schematic view of the time evolution of the hydrogen concentration across the membrane.

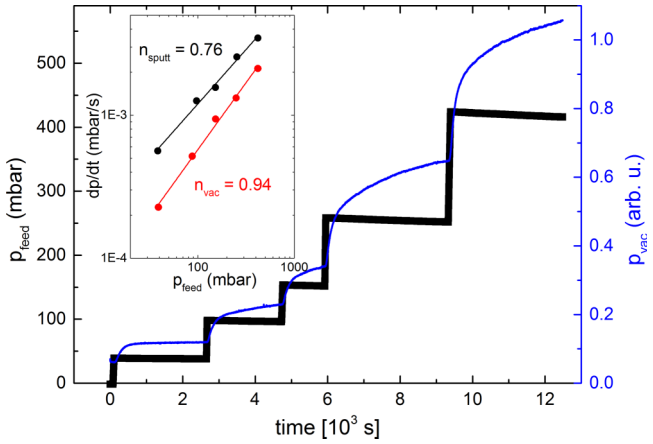

FIG. 3. Time evolution of p_{feed} and p_{vac} while imposing small pressure steps on the membrane feed side. Inset: derivation of n measured after 30 min sputtering with 3×10^{-6} mbar Ar (n_{sputt}) and after long-term storage at approximately 10^{-7} mbar (n_{vac}).

- Molecular hydrogen dissociates at the high-pressure surface of the membrane ("feed"), before diffusing through the membrane.
- Hydrogen atoms recombine at the low-pressure surface.
- The pressure difference is the thermodynamic driving force; the kinetic constraints are the adsorption, diffusion, and desorption processes (see the inset of Fig. 2).

With our setup, we can measure and manipulate the individual kinetic processes, giving us a tool to investigate the underlying material properties and to improve membrane systems. The functionality is best explained by measurements, which were carried here out on a 100 μm-thick Pd membrane (see Fig. 2). The p_{feed} value is increased from zero to the desired measurement pressure (here 420 mbar) and the corresponding valve is then closed. The hydrogen flux through the feed side of the membrane is measured by the pressure drop in the pressure system: $j = \Delta V/\Delta t\ 1/A = \Delta p/\Delta t\ V_0/A$. Here, V_0 is the volume of the pressure system and A is the area of the membrane. The measured curve approaches asymptotically a linear function, that is, j is constant for $t \geq \infty$. When the linear fit, which is fitted to the measurement data at large t values, is subtracted from the data, we are left with an exponential function. The exponential function is an approximation of the sorption function, that is, the time dependence of the uptake of hydrogen by the membrane (p_{ab}). Its half time, $t_{1/2} = 220$ s, is directly linked to the diffusion parameter of hydrogen in the membrane: $D = 0.0049/(t_{1/2}\ l^2)$,[14] giving $D = 1.4\ \times10^{-6}$ cm^2/s, which is in good agreement with previously reported data (ca. 3×10^{-6} cm^2/s at $T = 373$ K[15]). The hydrogen partial pressure inside the UHV chamber (p_{vac}, measured by mass spectrometry) is linked to the flux of hydrogen from the membrane by considering that it is proportional to the pumping speed of the attached turbo-molecular pump. Indeed, fitting the data to exponential curves gives the same half time (both when finite and zero pressures are applied to the feed side), as obtained from the pressure dependence of the feed side.

Additional conclusions are drawn from experiments in which the pressure is increased in small steps, yielding a pressure dependence of the hydrogen permeation (Fig. 3). Using classical kinetics theory, the pressure dependence of the flux is $j \sim p^n$, with n defining the rate-limiting step, that is, $n = 1$ for surface-controlled and $n = 1/2$ for diffusion-controlled processes.[16] As an example, we compare the very same Pd membrane, once measured after 30 min sputtering with 3×10^{-6} mbar Ar (j_{sputt}) and once after long-term storage at approximately 10^{-7} mbar (j_{vac}). A double-log plot gives $n_{sputt} = 0.76$, that is, a diffusion-controlled process, whereas $n_{vac} = 0.94$, that is, a surface-controlled process. A clean Pd membrane is indeed expected to exhibit diffusion-controlled kinetics at room temperature,[17] whereas a surface partially covered with impurities will slow down the desorption process.[18]

In both cases, the measurements suggest high hydrogen coverage of the low-pressure surface. We utilised XPS to measure the as-cleaned Pd membrane at different p_{feed} values to confirm this hypothesis. Fig. 4(a) shows the Pd 3d region at the start and at the end of the experiment, that is, before the first H_2 introduction step and at the last pressure step ($p_{feed} = 1$ bar). According to Schlapbach and Burger,[19] the chemical shift of the Pd 3d peak from Pd to Pd–H is 0.15 eV. This value is too small to obtain two distinct peaks; however, it is large enough for the overall shift of the Pd 3d peaks to be detected. We chose to fit the Pd $3d_{3/2}$ and Pd $3d_{5/2}$ components of the first spectrum, taken without any hydrogen on the membrane surface, each with one single peak. In addition to the clean Pd peak, a second peak was added to the fit, which was located 0.15 eV further towards higher apparent binding energies, accounting for Pd–H (Ref. 19). At a feed pressure of 1000 mbar, more than half of the total peak area corresponds to palladium hydride, that is, about 65% of the surface and sub-surface sites are filled with hydrogen. Fig. 4(b) shows that it is also possible to track the hydrogen concentration—extracted by standard XPS quantitative analysis[13]—as a function of p_{feed}, thereby enabling us to record a pressure–composition isotherm by means of XPS. The deviation from the bulk isotherm (taken from Ref. 20) comes partly from the fact that the microstructure of the Pd membrane considered here differs from that of a perfect bulk Pd specimen. Thin layers are indeed known to

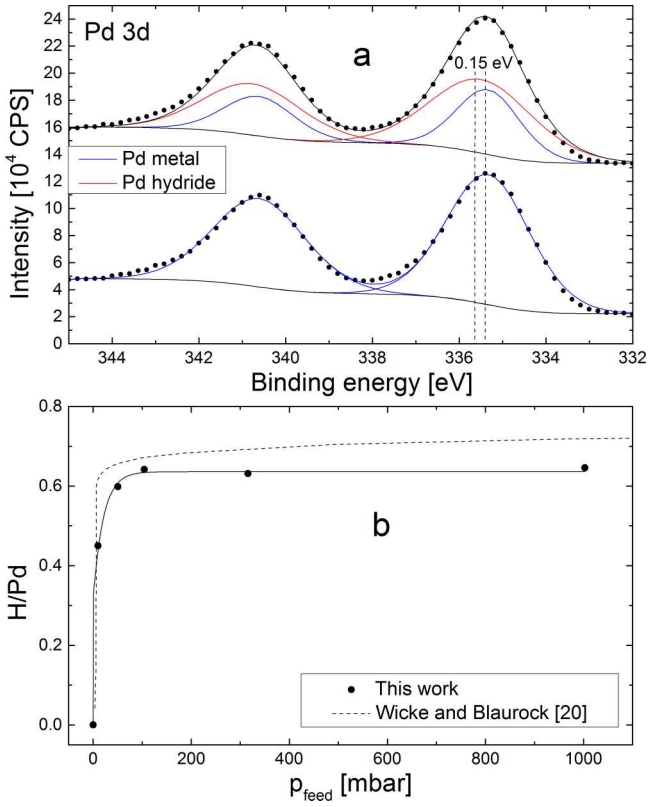

FIG. 4. (a) Pd 3d region of a pure Pd membrane (two scans, energy step: 0.2 eV) before the first H_2 introduction step (bottom) and at $p_{feed} = 1$ bar (top). (b) H/Pd atomic ratio as a function of p_{feed}, as extracted from XPS spectra. A classic bulk isotherm is displayed for comparison.

exhibit narrow and sloped miscibility gaps.[21] The XPS signal also contains a significant contribution from surface and subsurface sites, which are energetically very different from bulk sites.[22] However, a complete study of the Pd–H phase diagram is out of the scope of the present work.

This simple experiment confirms that the observation of palladium hydride by XPS is possible when using the present experimental approach, without having to cool to cryogenic temperatures and/or without using a differentially pumped approach. Furthermore, under specific conditions, the hydrogen coverage of the low-pressure surface corresponds to that of the feed side, enabling the study of hydrogenation reactions by UHV methods. The explanation is straightforward: if the low-pressure side of the Pd membrane is blocked by a coating, the hydrogen concentration directly under the coating equals exactly that of the concentration at the opposite (feed) side; in other words, we can measure reactions corresponding to 1 bar hydrogen by UHV methods (see Sec. IV).

The temperature dependence of the permeation kinetics also provides information about the membrane surface-hydrogen content. Such experiments are detailed in the supplementary material.[42] Figure 5 shows the hydrogen flux through a $Pd_{0.7}Ag_{0.3}$ membrane as a function of $1/T$. The 0.2 eV activation energy obtained between 140 and 160 °C is consistent with the 0.25 eV activation energy for hydrogen diffusion in $Pd_{0.7}Ag_{0.3}$, as measured by Wang *et al.*[23] The apparent activation energy then markedly increases around 130 °C, which is in agreement with the data from Okazaki *et al.*[24]

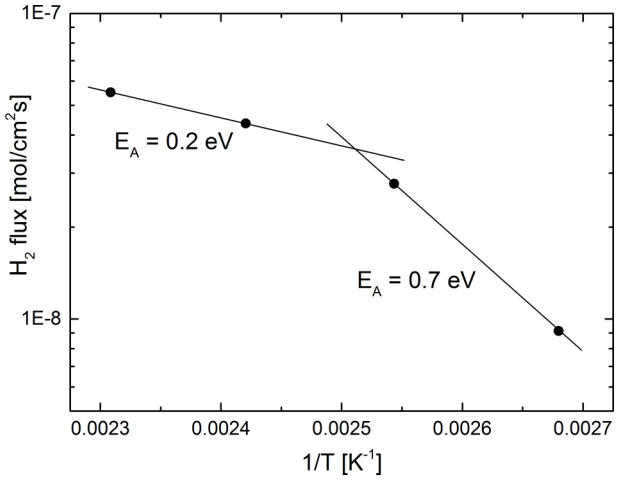

FIG. 5. Hydrogen flux as a function of $1/T$ for a $Pd_{0.7}Ag_{0.3}$ membrane.

The activation energy for hydrogen desorption is a function of the surface coverage, starting from about 1 eV for an empty surface and decreasing to about 0.4 eV when the surface coverage approaches unity.[17,25] Our value of 0.7 eV, obtained between 100 and 120 °C, therefore suggests a high surface coverage, although it is not equal to 1.

Studying the $Pd_{0.7}Ag_{0.3}$ composition also enables us to use the standard Ag $3d_{5/2}$ line for sensitivity and resolution measurements (a detailed report is available in the supplementary material[42]). In this context, our experimental approach does not differ from a classic XPS system, as the pressure reached in the AC is, at worst, on the order of 10^{-7} mbar for H_2 pressures up to 1 bar on the membrane feed side.

IV. EXAMPLE APPLICATIONS

Two applications of our *in situ* XPS approach will be presented in this section. The reduction of cobalt nitrate—a catalyst precursor for CO_2 hydrogenation—at room temperature will first be demonstrated, which involves the deposition of a material on the membrane surface. The second application will then focus on the hydrogenation of a WRC for photocatalytic H_2 production.

A. Reduction of cobalt nitrate

Cobalt is intensively studied as a catalyst in the form of metal nanoparticles or metal complexes for the electro-[26] or photoreduction[27] of CO_2 for the production of sustainable fuels. More specifically, Co catalysts are particularly well suited for the so-called Fischer–Tropsch synthesis.[28] The activation of Co nanoparticles for this process implies the calcination of the cobalt nitrate precursor at around 550 °C and the reduction of the subsequently formed cobalt-oxide phases under a hydrogen flow at around 400 °C (with pure hydrogen).[29] These conditions are too harsh for classic *in situ* XPS. In this section, we demonstrate that the present XPS technique has been applied to the cobalt nitrate precursor in order to (i) check if this compound could be directly reduced in an UHV with monoatomic hydrogen diffusing through a membrane and (ii) to capture potential reaction intermediates *in situ*.

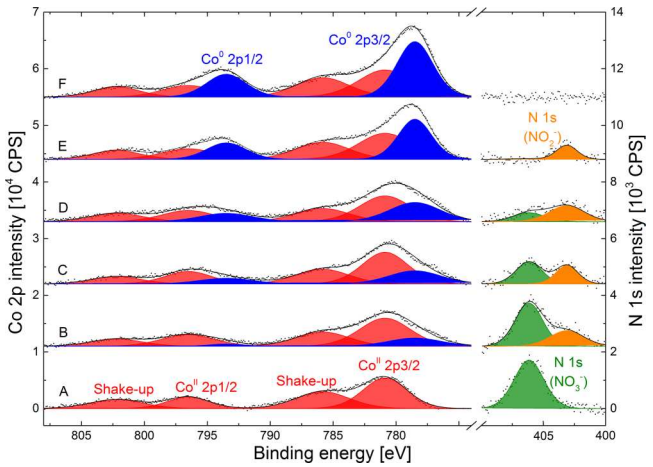

FIG. 6. Co 2p and N 1s regions (ten scans, energy step: 0.1 eV) of a $Co(NO_3)_2{\cdot}6H_2O$ layer deposited on a $Pd_{0.7}Ag_{0.3}$ membrane and submitted to the following conditions: (a) dehydrated for 3 days under UHV; then, p_{feed} is set to 465.5 mbar and the spectra were acquired after (b) 20 min, (c) 3 days, and (d) 10 days. (e) H_2 was then pumped from the feed side and the membrane was heated to 140 °C. (f) Two days after p_{feed} were set to 503.9 mbar at 140 °C.

Cobalt nitrate hexahydrate [$Co(NO_3)_2{\cdot}6H_2O$] from Sigma-Aldrich was dissolved in ethanol, and the UHV side of a 150 μm-thick $Pd_{0.7}Ag_{0.3}$ membrane was then coated with the solution. After evaporation of the solvent, the XPS system was pumped to UHV (without bake-out) and the specimen was dehydrated for 3 days. Spectrum A in Fig. 6 shows that the resulting deposit is indeed $Co(NO_3)_2$, with Co $2p_{3/2}$ at 780.9 eV (satellite at 785.8 eV) and Co $2p_{1/2}$ at 796.5 eV (satellite at 802.2 eV). These values are in good agreement with the data from Strydom.[30] However, one cannot exclude other Co(II) compounds, such as $Co(OH)_2$ and CoO, to be at least partly formed on the surface, as the XPS lines of these compounds are very close to those of $Co(NO_3)_2$.[31] The relative proportion of each Co(II) species could also change during the reduction process. Consequently, the red peaks in Fig. 6 will be assigned to a particular oxidation number [Co(II)], rather than one single compound, in order to simplify the situation and to avoid any peak fitting artefacts. On the contrary, both Co 2p peaks that are characteristic of Co metal are located more than 2 eV away from the Co(II) species cited above, making Co metal identifiable, without doubt. It should also be mentioned that the most intense peaks identified during this experiment were those of Pd and Ag from the supporting membrane, showing that the deposit was not thicker than a few nanometres.

After the acquisition of spectrum A under UHV, p_{feed} was set to 465.5 mbar. After 20 min at room temperature, 12.5% of the surface Co atoms had been reduced to Co(0). This number rises to 31.4% after 10 days. The remaining hydrogen was then flushed from the feed side and the membrane was heated to 140 °C. More cobalt was then reduced—most likely by a purely thermal effect—although probably aided by the solid hydrogen remaining in the membrane, up to a total of 38.2%. The p_{feed} was then set to 503.9 mbar, bringing the total percentage of reduced surface Co atoms to 45% after 2 additional days. As explained above, the remaining Co(II) species are likely to be cobalt oxide or hydroxide.

Additionally, although the N 1s peak observed for the as-deposited compound at 406.1 eV is characteristic of the NO_3^- ion,[32,33] another peak appears at 403.1 eV in spectrum (b), which further develops as the primary peak progressively vanishes (between spectra (b) and (d) in Fig. 6). If we consider the direct reduction of $Co(NO_3)_2$ to Co, then we can assign this new species to N_2O, which is in agreement with the data of Pashutski and Folman.[34] However, according to the same authors, N_2O can only be observed by XPS on such a metal surface at 80 K. We would then rather assign it to the NO_2^- ion.[35] We claim here that cobalt nitrite is a reaction intermediate, as it could only be stabilised by a counter ion such as K or Na. This statement is also supported by the decline of the second N 1s peak as the reaction advanced at room temperature (between spectra D and E in Fig. 6) and by the absence of any nitrogen species at 140 °C (spectrum (f) in Fig. 6). Therefore, we propose the following two-step mechanism for cobalt nitrate reduction by monoatomic hydrogen:

$$Co(NO_3)_2 + 4H \Leftrightarrow Co(NO_2)_2 + 2H_2O, \quad (1)$$

$$Co(NO_2)_2 + 8H \Leftrightarrow Co + 4H_2O + N_2. \quad (2)$$

More investigations will be carried out in order to validate this mechanism, which could be relevant to the field of Co catalysis. However, this is out of the scope of the present paper. It has been shown here that the present experimental approach can be successfully conducted in order to study the hydrogenation of deposits.

B. Hydrogenation of a water reduction catalyst

Surface solid–hydrogen interactions are also of primary importance for photo- and electrocatalytic H_2 production processes, in which the state-of-the-art catalyst focuses on the development of complex WRCs based on earth-abundant elements such as Co, Ni, and Fe.[1] In these processes, the central metallic element in the WRC is expected to reversibly change its oxidation state through successive electron transfers with a photosensitiser and water,[36] with the subsequent formation of intermediate forms of the WRC. Cobalt dioxime complexes are seen as promising catalysts in this respect, both regarding photo-[36] and electrocatalytic[37] H_2 production. We will focus here on such a compound with the formula $C_{18}H_{23}CoN_6O_4$ (see Fig. 7); the documentation of this compound can be found elsewhere (see compound 10 in Ref. 38). This compound has been shown by Probst *et al.* to form a hydride intermediate during photocatalytic H_2 formation.[38] Initially, the cobalt oxidation state changes from +III to +II, according to reaction A in Fig. 7, through reduction by a photogenerated reductant. This is then followed by the loss of an axial pyridine ligand. Further reduction gives penta-coordinated Co(I), which can be protonated on cobalt to give the Co(III)–H species—the key intermediate in H_2 formation. This WRC is the performance-limiting compound in the water-splitting system proposed by Probst *et al.*, in terms of H_2 turnover frequency. Furthermore, its long-term efficiency is affected by a deactivation process; the investigation of this would help to develop more stable catalysts, according to the same authors.[38]

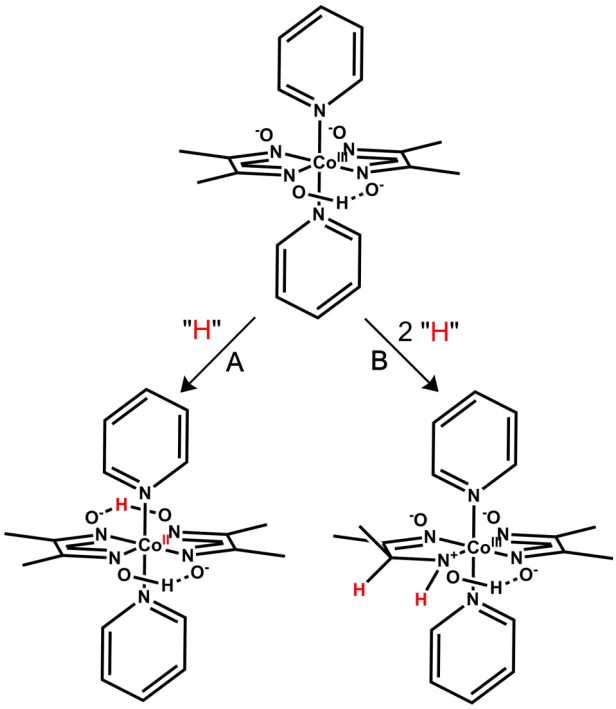

FIG. 7. Two hydride-formation paths of a Co-based WRC. (a) Initial reduction of Co(III) to Co(II) (see Ref. 38). (b) Unwanted deactivation process.

Here, we have used our *in situ* XPS approach to identify possible hydride forms of the WRC described above, together with experimental conditions required to favour a given product. The WRC was dissolved in CH_2Cl_2, and the UHV side of a 100 μm-thick Pd membrane was then coated with the solution. After evaporation of the solvent, the XPS system was pumped to UHV (again without bake-out). The C 1s region shown in Fig. 8(a) confirms that this complex molecule retained its structure upon deposition. Indeed, the following restrictions have been imposed to the three components of this fit. First, the latter have been ranked in terms of apparent binding energies, with respect to the expected electron densities of the carbons atoms,[39,40] that is, from highest to lowest: methyl groups, pyridine carbons (together with their π–π^* transition characteristic of aromatic rings[41]), and dioxime carbons. Second, the areas of these peaks were forced to fit with the concentration of each carbon in the molecule (e.g., the area of the red peak in Fig. 8(a) is equal to 2/9 times the total C 1s area).

Increasing H_2 pressures were then imposed on the membrane feed side at room temperature. Despite the very small binding-energy shift of Co 2p (see Fig. 8(c)), the only atom that changed its electron density significantly was nitrogen (see Fig. 8(b)). Although the N 1s compound observed before hydrogen exposure at 401 eV—which includes here the pyridine and the dioxime nitrogen atoms, as they exhibit similar chemical environments—decreases upon hydride formation, another compound develops at 399.1 eV. If hydrogen binds to the dioxime nitrogen atoms, as indicated in reaction B of Fig. 7, it will then indeed appear at a lower apparent binding energy. The maximum concentration of nitrogen reduced this way is equal to 44.9%, that is, 67.4% of the dioxime nitrogen. Probst *et al.* previously identified this unwanted hydride-formation path as a potential deactivation process for this WRC.[38]

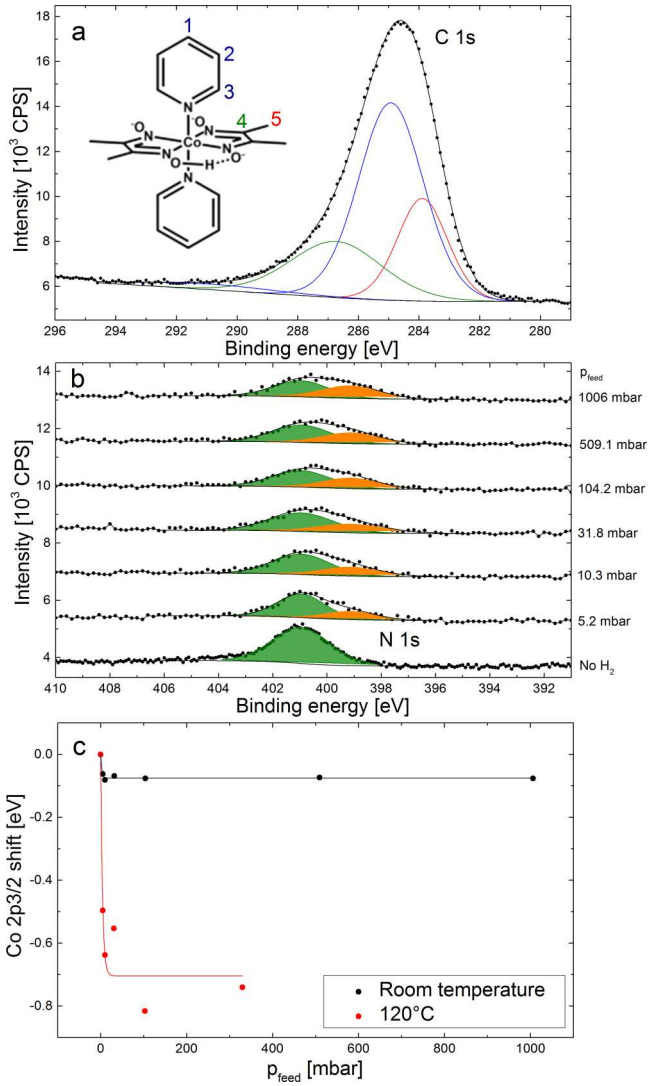

FIG. 8. (a) C 1s region of the WRC described in Fig. 7 deposited on a pure Pd membrane (ten scans, energy step: 0.1 eV). (b) N 1s region of the WRC (ten scans, energy step: 0.2 eV) at room temperature with the membrane feed side exposed to different H_2 pressures. (c) Co $2p_{3/2}$ binding energy shift as a function of the H_2 pressure on the feed side.

The same hydride formation experiment was then reproduced at 120 °C. Interestingly, the N 1s signal does not evolve anymore at this temperature, but cobalt is reduced according to reaction A in Fig. 7, as indicated by the evolution of the Co $2p_{3/2}$ shift in Fig. 8(c). We show here that the deactivating hydride mechanism (reaction B) is favoured over the hydride mechanism of reaction A, which can only be observed after reaction B is at equilibrium and upon heating to a temperature that is inappropriate for photocatalytic hydrogen production. The structure of this WRC could be modified in the future, according to these conclusions.

V. CONCLUSIONS AND OUTLOOK

This paper presents a cheap and high-performance alternative to classic differential pumping and low-temperature approaches for studying hydrogen–solid interactions by means of XPS. Its simple design, inspired by well-established membrane

technology, is adaptable to any XPS setup. It could also serve other types of UHV-based *in situ* techniques in the future. This setup will be of great use in membrane science in order to obtain the rate-limiting step of permeation in new membranes, as well as the role of its surface properties. Furthermore, if a membrane with known properties (Pd) is used and a novel material is deposited onto it, we have quantitative access to hydrogenation reaction kinetics, intermediates, and products as well as its surface properties, which provide crucial information for energy materials, catalysts, etc.

We have demonstrated the proof-of-concept by modelling the hydrogen permeation mechanism through the membrane specimen holder with classical diffusion theory. At a given membrane thickness, the rate-limiting step is not only a function of temperature but also depends on surface contaminants. Either way, high hydrogen surface coverage on the low-pressure membrane side can be reached by adjusting the pressure on the feed side. Moreover, when a deposit is present on the surface of the feed side, it slows down or even blocks the permeation mechanism, thereby further increasing the surface hydrogen content. The presence of the membrane specimen holder does not significantly affect the spectrometer sensitivity or energy resolution, even at $p_{\text{feed}} = 1$ bar.

Two different deposits were used to validate this new setup. We conducted the reduction of cobalt nitrate with monoatomic hydrogen at relatively low temperatures compared to classic preparation methods for CO_2 hydrogenation catalysts. A two-step mechanism was proposed in this respect. The importance of understanding the deactivation mechanisms by hydrogen for WRCs was also pointed out. We unravelled a preferential hydride formation mechanism for the WRC studied herein, which is responsible for its limited H_2 turnover frequency.

So far, we have only validated hydrogen as the surface-interacting gas to act as the alternative to differential pumping. However, by using different types of membranes, we aim to adapt the present experimental approach to other gases in the future.

ACKNOWLEDGMENTS

This work was partly supported by the European Commission, Grant Agreement No. FP7–284522 (infrastructure program H2FC), the UZH-UFSP program LightChEC, and by CCEM and Swisselectric research through the HyTech project. We warmly acknowledge Urs Hintermüller from the Mechanical Engineering Department at Empa for his help in the design of the membrane specimen holder.

[1]P. Du and R. Eisenberg, Energy Environ. Sci. **5**, 6012–6021 (2012).
[2]S. N. Riduan and Y. Zhang, Dalton Trans. **39**, 3347–3357 (2010).
[3]J. von Pezold, L. Lymperakis, and J. Neugebeauer, Acta Mater. **59**, 2969–2980 (2011).
[4]B. Sakintuna, F. Lamari-Darkrim, and M. Hirscher, Int. J. Hydrogen Energy **32**, 1121–1140 (2007).
[5]B. Sundqvist, Solid State Phenom. **150**, 175–195 (2009).
[6]D. Teichmann, W. Arlt, P. Wasserscheid, and R. Freymann, Energy Environ. Sci. **4**, 2767–2773 (2011).
[7]F. Mangolini, J. B. Åhlund, G. E. Wabiszewski, V. P. Adiga, P. Egberts, F. Streller, F. Backlund, P. G. Karlsson, B. Wannberg, and R. W. Carpick, Rev. Sci. Instrum. **83**, 093112 (2012).
[8]M. Salmeron and R. Schlögl, Surf. Sci. Rep. **63**, 169–199 (2008).
[9]H. Bluhm, J. Electron Spectrosc. Relat. Phenom. **177**, 71–84 (2010).
[10]M. E. Grass, P. G. Karlsson, F. Aksoy, M. Lundqvist, B. Wannberg, B. S. Mun, Z. Hussain, and Z. Liu, Rev. Sci. Instrum. **81**, 053106 (2010).
[11]A. Jürgensen, N. Esser, and R. Hergenröder, Surf. Interface Anal. **44**, 1100–1103 (2012).
[12]F. F. Tao, Chem. Commun. **48**, 3812–3814 (2012).
[13]N. Fairley and A. Carrick, *The Casa Cookbook–Part 1: Recipes for XPS Data Processing* (Acolyte Science, Knutsford, 2005).
[14]J. Crank, *The Mathematics of Diffusion*, 2nd ed. (Oxford University Press, Oxford, 1975), pp. 238–239.
[15]J. Völkl and H. Wipf, Hyperfine Interact. **8**, 631–637 (1981).
[16]A. Borgschulte, R. Gremaud, and R. Griessen, Phys. Rev. B **78**, 094106 (2008).
[17]T. L. Ward and T. Dao, J. Membr. Sci. **153**, 211–231 (1999).
[18]J. Hulme, M. Komaki, C. Nishimura, and J. Gwak, Curr. Appl. Phys. **11**, 972–975 (2011).
[19]L. Schlapbach and J. P. Burger, J. Phys. Lett. **43**, L273–L276 (1982).
[20]E. Wicke and J. Blaurock, J. Less-Common Met. **130**, 351–363 (1987).
[21]R. J. Westerwaal, C. den besten, M. Slaman, B. Dam, D. E. Nanu, A. J. Böttger, and W. G. Haije, Int. J. Hydrogen Energy **36**, 1074–1082 (2011).
[22]S. Hong and T. S. Rahman, Phys. Rev. B **75**, 155405 (2007).
[23]D. Wang, T. B. Flanagan, and K. Shanahan, J. Phys. Chem. B **112**, 1135–1148 (2008).
[24]J. Okazaki, D. A. P. Tanaka, M. A. L. Tanco, Y. Wakui, F. Mizukami, and T. M. Suzuki, J. Membr. Sci. **282**, 370–374 (2006).
[25]M. Johansson, E. Skúlason, G. Nielsen, S. Murphy, R. M. Nielsen, and I. Chorkendorff, Surf. Sci. **604**, 718–729 (2010).
[26]R. J. Lim, M. Xie, M. A. Sk, J.-M. Lee, A. Fischer, X. Wang, and K. H. Lim, Catal. Today **233**, 169–180 (2014).
[27]T. Jin, C. Liu, and G. Li, Chem. Commun. **50**, 6221–6224 (2014).
[28]K. M. Cook, S. Poudyal, J. T. Miller, C. H. Bartholomew, and W. C. Hecker, Appl. Catal., A **449**, 69–80 (2012).
[29]B. Ernst, S. Libs, P. Chaumette, and A. Kiennemann, Appl. Catal., A **186**, 145–168 (1999).
[30]C. A. Strydom and H. J. Strydom, Inorg. Chim. Acta **159**, 191–195 (1989).
[31]B. J. Tan, K. J. Klabunde, and P. M. A. Sherwood, J. Am. Chem. Soc. **113**, 855–861 (1991).
[32]C. A. Tolman, W. M. Riggs, W. J. Linn, C. M. King, and R. C. Wendt, Inorg. Chem. **12**, 2770–2778 (1973).
[33]V. K. Kaushik, J. Electron Spectrosc. Relat. Phenom. **56**, 273–277 (1991).
[34]A. Pashutski and M. Folman, Surf. Sci. **216**, 395–408 (1989).
[35]B. Folkesson, Acta Chem. Scand. **27**, 287–302 (1973).
[36]B. Probst, A. Rodenberg, M. Guttentag, P. Hamm, and R. Alberto, Inorg. Chem. **49**, 6453–6460 (2010).
[37]P.-A. Jacques, V. Artero, J. Pécaut, and M. Fontecave, Proc. Natl. Acad. Sci. U. S. A. **106**, 20627–20632 (2009).
[38]B. Probst, M. Guttentag, A. Rodenberg, P. Hamm, and R. Alberto, Inorg. Chem. **50**, 3404–3412 (2011).
[39]B. Mustafa, N. Md Gabra, P. Nagababu, and S. Satyanarayana, J. Chem. Pharm. Res. **3**, 968–981 (2011).
[40]S. C. Nayak, P. K. Das, and K. K. Sahoo, Chem. Pap. **57**, 91–96 (2003).
[41]J. M. González-Domínguez, P. Castell, S. Bespín-Gascón, A. Ansón-Casaos, A. M. Díez-Pascual, M. A. Gómez-Fatou, A. M. Benito, W. K. Maser, and T. M. Martínez, J. Mater. Chem. **22**, 21285–21297 (2012).
[42]See supplementary material at http://dx.doi.org/10.1063/1.4921353 for temperature dependence and XPS spectra.